

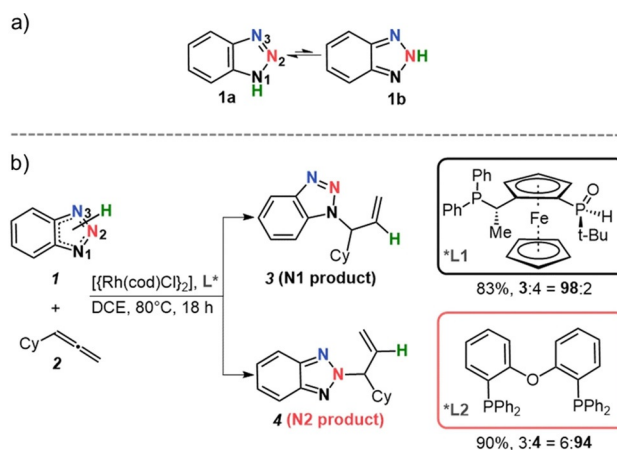
Allylation

Ligand-Mediated Regioselective Rhodium-Catalyzed Benzotriazole–Allene Coupling: Mechanistic Exploration and Quantum Chemical Analysis

Tetiana Sergeieva,^[a, b] Trevor A. Hamlin,^[b] Sergiy Okovytyy,^[c] Bernhard Breit,^{*,[a]} and F. Matthias Bickelhaupt^{*,[b, d]}

Abstract: The ligand-controlled rhodium-catalyzed regioselective coupling of 1,2,3-benzotriazoles and allenes was investigated by DFT calculations. Because allylation can occur at either the N1 or N2 position of the 1,2,3-benzotriazole, the complete Gibbs free energy profiles for both pathways were computed. A kinetic preference emerged for the experimentally observed N1 allylation with the Jo-SPOphos ligand, whereas N2 allylation was favored with DPEphos. Analysis of the regiodetermining oxidative addition step by using the activation strain model in conjunction with a matching energy decomposition analysis has revealed that the unprecedented N2 reaction regioselectivity is dictated by the strength of the electrostatic interactions between the 1,2,3-benzotriazole and the rhodium catalyst. The nature of the electrostatic interaction was rationalized by analysis of the electrostatic potential maps and Hirshfeld charges: a stabilizing electrostatic interaction was found between the key atoms involved in the oxidative addition for the N2 pathway, analogous interactions are weaker in the N1 case.

Controlling the regioselectivity of fundamental organic transformations is an outstanding challenge in synthesis.^[1] The N-selective functionalization of 1,2,3-benzotriazoles is a particular challenge due to the dynamic equilibrium between two tautomeric forms of the benzotriazole (Scheme 1 a).^[2] Despite of the greater stability of tautomer **1 a**, alkylation of 1,2,3-benzotriazole has typically been observed to be moderately selective at N1/N3 position and extremely unselective at N2.



Scheme 1. (a) Tautomeric equilibrium of 1,2,3-benzotriazole; (b) Synthetic protocol of regioselective Rh catalyzed addition of 1,2,3-benzotriazoles to allenes.

Major advances have been forged for N1-selective methods.^[3] N2-selective modification is underdeveloped, primarily because of difficulties in shifting the equilibrium toward **1 b** tautomer. As a consequence, the structural space around valuable N2-substituted 1,2,3-benzotriazoles that often occur in pharmaceutical agents, agrochemicals and advanced materials is limited.^[3,4]

The rare examples of N2 procedures reported during the last decade mostly rely on structural modification of the coupling partners.^[3] These methods are usually based on sterically bulky groups on the benzotriazole or alkylating agent that block access to the terminal nitrogens N1/N3, thereby making the N2 position the preferred site of nucleophilic attack. Despite being practically successful, these strategies are restricted in

[a] Dr. T. Sergeieva, Prof. Dr. B. Breit
Institute for Organic Chemistry, University of Freiburg
Albertstrasse 21, 79104, Freiburg im Breisgau (Germany)
E-mail: bernhard.breit@chemie.uni-freiburg.de

[b] Dr. T. Sergeieva, Dr. T. A. Hamlin, Prof. Dr. F. M. Bickelhaupt
Department of Theoretical Chemistry, Amsterdam Center for Multiscale Modeling (ACMM), Vrije Universiteit Amsterdam
De Boelelaan 1083, 1081 HV Amsterdam (The Netherlands)
E-mail: f.m.bickelhaupt@vu.nl

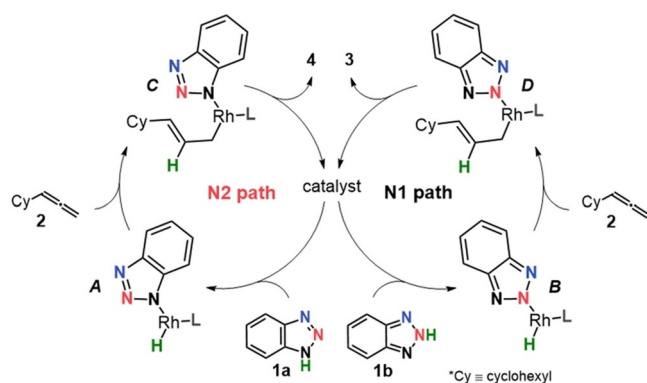
[c] Prof. Dr. S. Okovytyy
Department of Chemistry, Oles Honchar Dnipro National University
72 Gagarina Avn., 49000, Dnipro (Ukraine)

[d] Prof. Dr. F. M. Bickelhaupt
Institute for Molecules and Materials (IMM), Radboud University
Heyendaalseweg 135, 6525 AJ Nijmegen (The Netherlands)

Supporting information and the ORCID identification number(s) for the author(s) of this article can be found under:
<https://doi.org/10.1002/chem.201905359>

© 2019 The Authors. Published by Wiley-VCH Verlag GmbH & Co. KGaA. This is an open access article under the terms of the Creative Commons Attribution License, which permits use, distribution and reproduction in any medium, provided the original work is properly cited.

functional-group tolerance and require prefunctionalized reactants. Transition-metal catalysis offers an alternative approach that circumvents these previously mentioned issues as it involves the direct activation of X–H bonds for functionalizing molecules. In 2014, we proposed an unprecedented rhodium (Rh) catalyzed allylation of 1,2,3-benzotriazoles. This methodology was attractive in the sense that it gave high N1/N2 regioselectivity and had a high tolerance toward a broad range of 1,2,3-benzotriazole and allene derivatives.^[5] Importantly, the N1 or N2 regioselectivity could be tuned by judicious choice of the ligand on the Rh center. Among a series of diphosphine ligands used for the initial screening, we found that JoSPOphos (L1) gave the preference of N1 product, whereas DPEphos (L2) gave exclusive formation of the desired N2 substituted benzotriazole (Scheme 1 b). Intrigued by this fact, we performed additional experiments^[5] to probe the reaction mechanism and proposed the catalytic cycle illustrated in Scheme 2. The reaction involves three steps and begins with oxidative addition of benzotriazole tautomers **1 a/b** to the Rh^I complex. The generated Rh^{III}–H intermediates A and B proceed through hydrometalation and transform into σ -allyl complexes C and D. Intermediates C or D then undergo reductive elimination with the concomitant release of N-allylated products **4** and **3**, respectively.



Scheme 2. Proposed reaction mechanism for Rh catalyzed coupling of 1,2,3-benzotriazoles with allenes.

Despite the plausibility of the reaction mechanism outlined in the Scheme 2, the factors determining the unusual N2 regioselectivity remain unclear. This fact has motivated us to study the reaction mechanism using density functional theory (DFT) calculations. To provide general concepts for the rational design of other complementary approaches for the regioselective synthesis of valuable N-substituted synthons, the following questions must be addressed: 1) What is the reaction mechanism? 2) Which step of the catalytic cycle is regiodetermining? 3) What are the physical factors behind the regioselectivity? To answer these questions, we have performed a systematic in-depth theoretical investigation based on the accounts of the previously reported experimental data.^[5]

The coordination of Rh to L1' was initially investigated to determine the active form of the catalyst. Figure 1 illustrates the two possible binding modes of the JoSPOphos ligand (L1') to

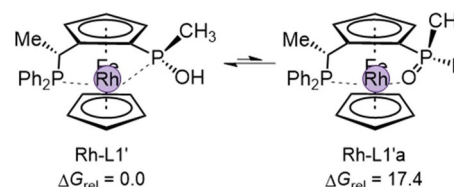
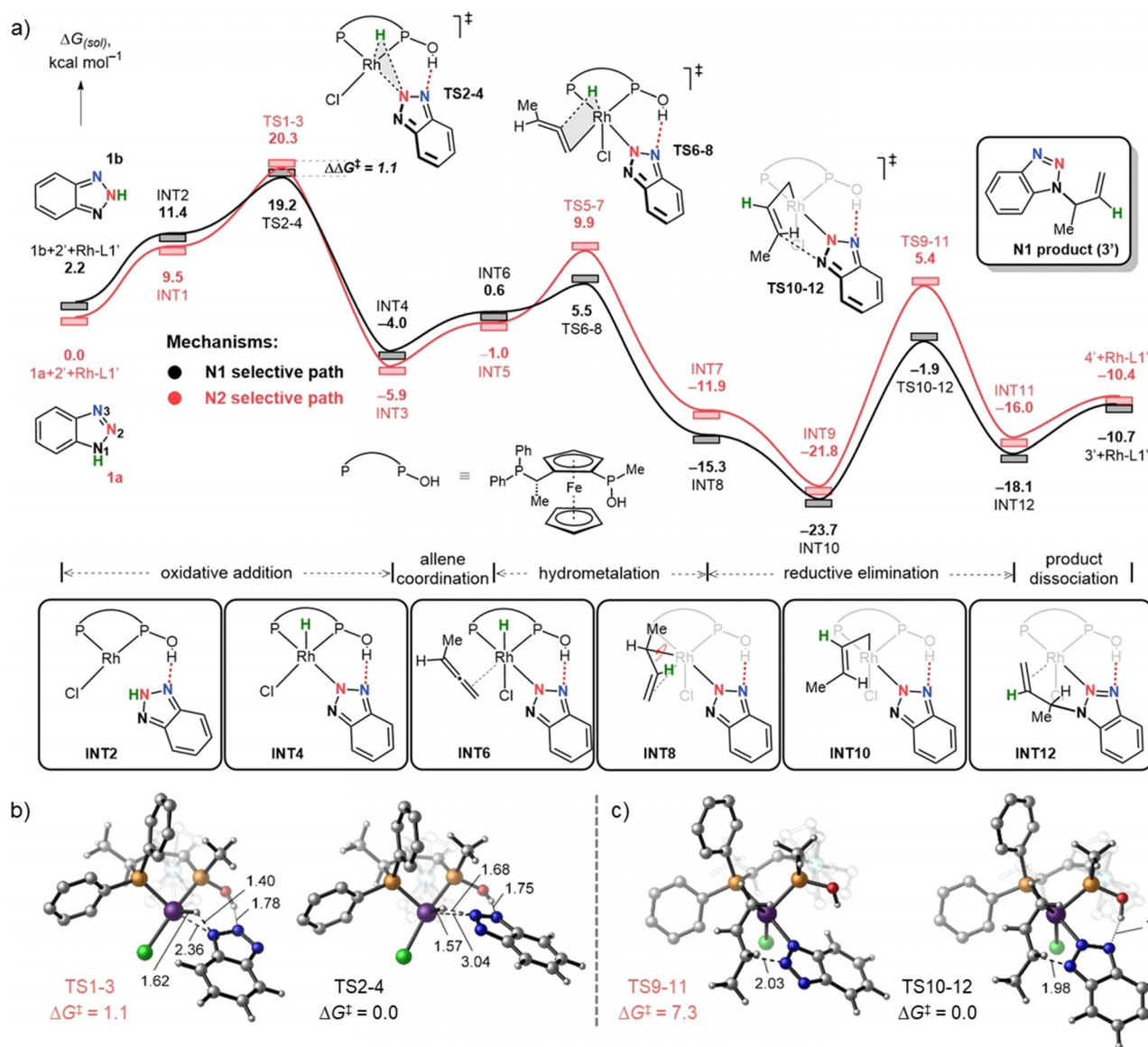


Figure 1. Coordination modes of L1' to the Rh. To reduce computational cost the *tert*-butyl group of the ligand (L1) was replaced with methyl (L1'). Relative energies [kcal mol⁻¹] were computed at SMD(DCE)-B3LYP-D3/6-31G(d)/LANL2DZ.

the Rh center.^[6] The large difference in computed Gibbs free energies ($\Delta\Delta G = 17.4$ kcal mol⁻¹) results from a favorable P-type of binding in Rh-L1'. Having determined the structure of the catalyst, we then investigated the reaction mechanism.

All relevant mechanistic pathways (for details, see the Supporting Information, Figure S1) were computationally^[7] explored and the Gibbs free energy profiles of the most favorable catalytic process were constructed (Scheme 3a). DFT calculations revealed a kinetic preference for N1 allylation (black color pathway) over N2, which is in line with experimental results of N1-substituted benzotriazole (**3**) being the major product when JoSPOphos is employed.

The reaction is initiated by coordination of the substrate **1 a/b** to Rh-L1' to form the pre-reactant complexes INT1 and INT2. Notably, the hydroxy group on the Rh-L1' catalyst acts as a directing group for the incoming benzotriazole and results in an OH...N1/N2 hydrogen-bonding interaction. Either the N1–H (**1 a** tautomer) or N2–H bond (**1 b** tautomer) can undergo oxidative addition depending on the tautomeric form of the benzotriazole. The oxidative addition involves the classical 3-membered TSs (TS1-3, TS2-4) with relative free energies of 20.3 and 19.2 kcal mol⁻¹. Computed structures of TS1-3 and TS2-4 are illustrated in Scheme 3b and reveal a late, product-like character for TS1-3 with a nearly formed Rh–N bond at 2.36 Å and an earlier TS structure for TS2-4, in which the Rh–N bond is still relatively long 3.04 Å. Because formation of INT3 and INT4 is downhill with respect to INT1, INT2 by 15.4 kcal mol⁻¹ in both cases, the oxidative addition step is predicted to be irreversible. To provide a coordination site necessary for the subsequent hydrometalation of the allene, the Cl ligand migrates to an axial position, whereas the allene binds to the Rh via an external C=C double bond in the equatorial plane. This ligand transformation raises energies to –1.0 and 0.6 kcal mol⁻¹ to form INT5 and INT6, respectively. The catalytic cycle continues with the hydrometalation and passes over transition states TS5-7, TS6-8 with Gibbs free activation barriers of 8.9 and 4.9 kcal mol⁻¹, respectively. The resulting intermediates INT7, INT8 are asymmetrical π -type complexes located at –11.9 and –15.3 kcal mol⁻¹, which further isomerize to more stable σ -allyl intermediates^[8] INT9, INT10 with relative free energies of –21.8 and –23.7 kcal mol⁻¹. The reductive elimination traversing transition states TS9-11, TS10-12 and affords the product complexes INT11, INT12. It is worth pointing out that the calculated activation barrier of reductive elimination for the N1-selective pathway (Scheme 3a, in black) is significantly lower ($\Delta\Delta G^\ddagger =$



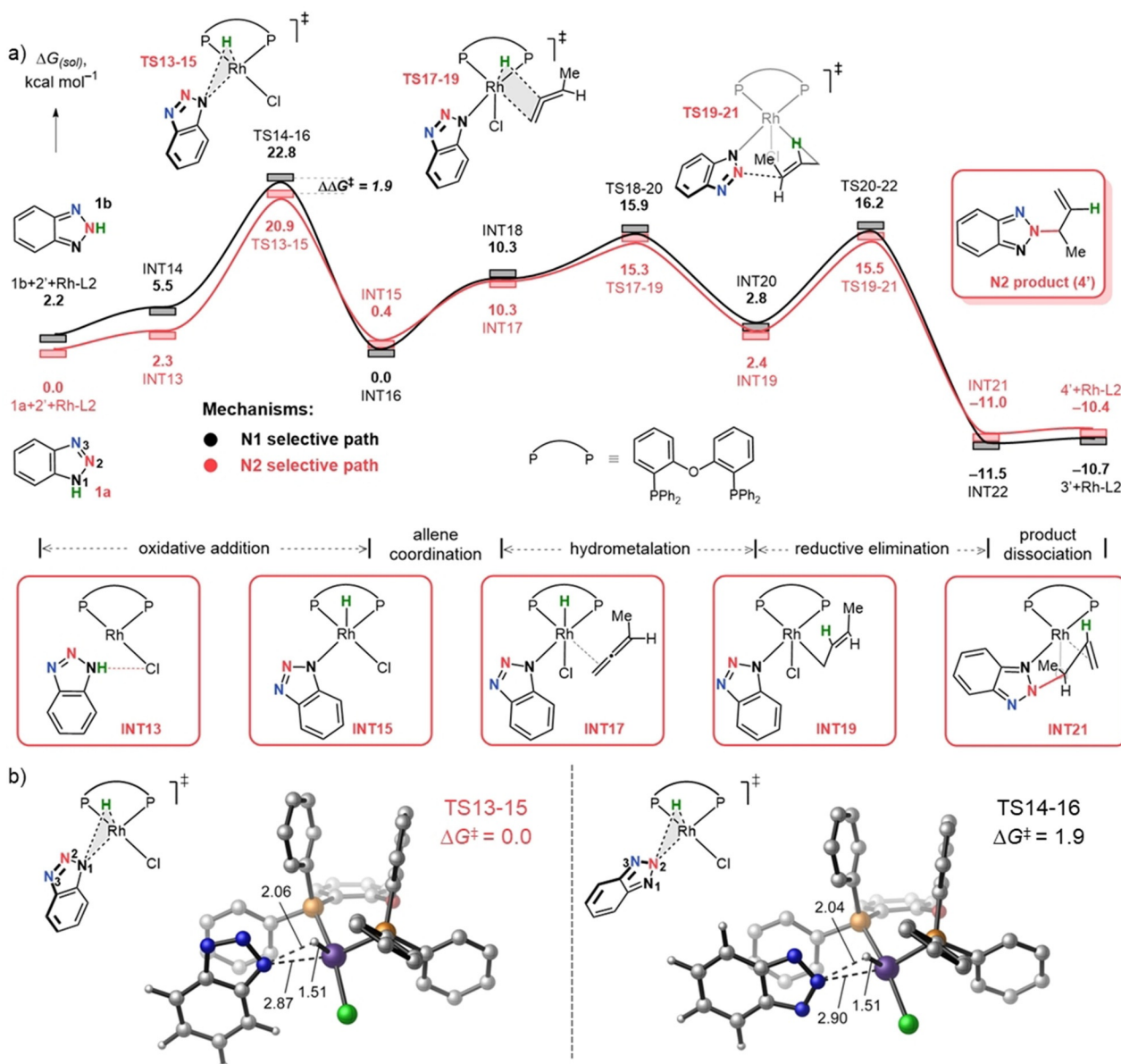
Scheme 3. (a) Gibbs free energy profile for coupling of the 1,2,3-benzotriazoles with allenes catalyzed by Rh-L1' at 80 °C and a standard state of 1 mol L⁻¹; (b) Regioselectivity determining transition states; (c) Rate-determining transition states. Bond lengths in Å, Gibbs free energies in kcal mol⁻¹. To reduce computational cost the cyclohexyl group of allene (2) was replaced by the methyl group (2') and *tert*-butyl group of the ligand (L1) was replaced with methyl (L1'). All data computed at SMD(DCE)-B3LYP-D3/6-311++G(d,p)/SDD//SMD(DCE)-B3LYP-D3/6-31G(d)/LANL2DZ.

5.4 kcal mol⁻¹) compared to the N2 route. The optimized transition structures (Scheme 3c) reveal a stabilizing hydrogen-bonding interaction in TS10-12 that is absent in TS9-11, which may be the origin of the lower barrier for the former. Release of products 3' and 4' allows the Rh catalyst to reenter the catalytic cycle and bind a new substrate. The Gibbs free energy profile provided in Scheme 3a reveals that the oxidative addition is the regioselectivity determining step, while the reductive elimination is the rate-determining step. Our DFT calculations support the experimental observation^[5] of N1-allylated regioisomer (3') being a preferred product as a TS2-4 associated with N1-selective path is more stable than a competitive TS1-3 for 1.1 kcal mol⁻¹.

To understand why simply changing the JoSPOphos ligand (L1) with DPEphos (L2) completely switches the regioselectivity

from N1 to N2, we again sampled various mechanistic possibilities (see the Supporting Information, Figures S2, S3) and outlined the lowest-energy reaction profiles corresponded to N1 and N2 pathways (Scheme 4a). In contrast to L1' (Scheme 3a), now the N2 reaction channel (red curve, Scheme 4a) is kinetically favored, which is in line with the experimental regioselective allylation at N2 atom of the benzotriazole.

The first elementary step of the catalytic cycle (Scheme 4a), namely, oxidative addition takes place from INT13 or INT14, in which the substrates 1a or 1b are pre-coordinated to the catalyst via a weak hydrogen-bond interaction between N1/2-H...Cl. From the substrate-coordinated complexes INT13 and INT14, the N1/N2-H activation is taking place via TS13-15/TS14-16 located at 20.9 and 22.8 kcal mol⁻¹. Optimized structures of TS13-15, TS14-16 are provided in Scheme 4b and are



Scheme 4. (a) Gibbs free energy profile for coupling of the 1,2,3-benzotriazoles with allenes catalyzed by Rh-L2 at 80 °C and a standard state of 1 mol L⁻¹; (b) Regioselectivity determining transition states. Bond lengths in Å, Gibbs free energies in kcal mol⁻¹. To reduce computational cost the cyclohexyl group of allene (2) was replaced by the methyl group (2'). All data computed at SMD(DCE)-B3LYP-D3/6-311++G(d,p)/SDD//SMD(DCE)-B3LYP-D3/6-31G(d)/LANL2DZ.

late with respect to the N–H bond breaking, displaying N–H distances of approximately 2.0 Å. The Rh^{III} hydride intermediates (INT15, INT16) furnished after the oxidative addition adopt a pentacoordinate structure bearing a hydride in the apical and benzotriazole fragment in the equatorial positions. The formation of these species is exergonic relative to the pre-reactive complexes (INT13, INT14) by 1.9 and 5.5 kcal mol⁻¹, respectively, suggesting oxidative addition to be irreversible. Binding of the incoming allene 2' during the second stage of the catalytic cycle is uphill in terms of Gibbs free energy by 9.9 (INT17) and 10.3 (INT18) kcal mol⁻¹. During this process, the coordination geometry at the Rh center changes from square pyramidal to octahedral, in which Cl and H ligands occupy apical positions. The reaction continues with a fast hydrometalation pro-

cess via TS17-19, TS18-20 with activation free energies of 6.0 and 6.9 kcal mol⁻¹ to give σ -allyl complexes (INT19, INT20). Finally, the hydrometalation adducts undergo reductive elimination with barriers of 13.1 and 13.4 kcal mol⁻¹ (TS19-21 and TS20-22), and deliver the product complexes INT21 and INT22. The catalytic cycle completes upon dissociation of the *N*-allylated products 3' or 4' from the coordination sphere of the metal with the regeneration of the catalyst. Considering the full Gibbs free energy profile illustrated in Scheme 4a, the key step determining the regioselectivity of the allylation is the oxidative addition step. Our DFT results show TS13-15 to be more stable than TS14-16 by 1.9 kcal mol⁻¹. This $\Delta\Delta G^\ddagger$ between the regiodetermining TSs corresponds to a ratio of N1/N2 4:96 with predominance of N2 allylated regioisomer 4', which is in

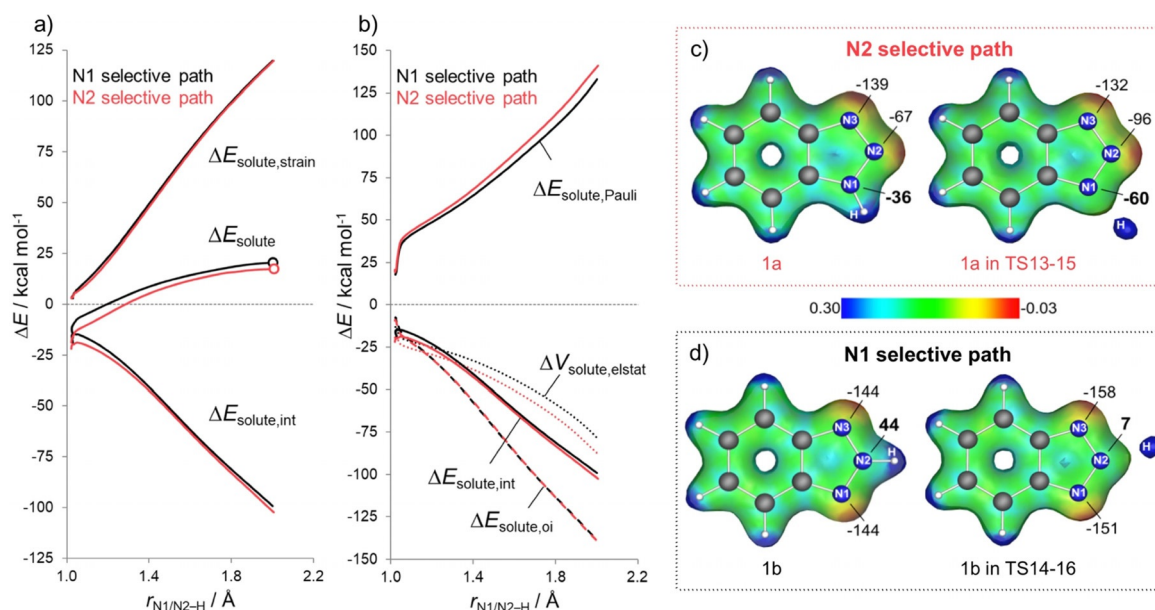


Figure 2. (a) Activation strain analyses and (b) energy decomposition analyses for the oxidative addition of 1,2,3-benzotriazole **1a** (N2-selective pathway) or **1b** (N1-selective pathway) to Rh-L2 computed at ZORA-B3LYP-D3/TZ2P level. Dots represent TSs. Electrostatic potential maps along with the Hirshfeld charges (m.a.u.) at N1, N2, N3 atoms of the 1,2,3-benzotriazole fragment (**1a/1b**) in both equilibrium (**1a/1b**) and transition state (TS13-15/TS14-16) geometries correspond to (c) N2- and (d) N1-selective pathways. ESP maps are plotted on the total electron density of the 1,2,3-benzotriazole fragment from the ZORA-B3LYP-D3/TZ2P calculations by using a consistent surface potential range of -0.03 a.u. to 0.30 a.u. and isovalue 0.045 .

perfect agreement with the experimentally isolated ratio of N1/N2 6:94.

To understand why DPEphos (L2) leads to N2 regioselectivity, we quantitatively analyzed the regiodetermining oxidative addition step catalyzed by Rh-L2 using the activation strain model ASM (Figure 2).^[9] Within the ASM, the relative energy in solution $\Delta E_{\text{solution}}$ along the reaction energy profile is separated into the energy of the solute ΔE_{solute} (reaction system in vacuum with the solution phase geometry) and the solvation energy $\Delta E_{\text{solvation}}$ [Eq. 1].

$$\Delta E_{\text{solution}} = \Delta E_{\text{solute}} + \Delta E_{\text{solvation}} \quad (1)$$

The intrinsic energy of the solute ΔE_{solute} is split further into two terms: $\Delta E_{\text{solute, strain}}$ (energy required for deformation of fragments from their starting geometries to the geometries they obtain over the course of the reaction) and $\Delta E_{\text{solute, int}}$ (energy of interaction between deformed fragments) [Eq. 2].

$$\Delta E_{\text{solute}} = \Delta E_{\text{solute, strain}} + \Delta E_{\text{solute, int}} \quad (2)$$

Next, the interaction energy $\Delta E_{\text{solute, int}}$ is decomposed into three terms using a canonical energy decomposition analysis (EDA) [Eq. 3]:

$$\Delta E_{\text{solute, int}} = \Delta V_{\text{solute, elstat}} + \Delta E_{\text{solute, Pauli}} + \Delta E_{\text{solute, oi}} \quad (3)$$

in which $\Delta V_{\text{solute, elstat}}$ corresponds to the electrostatic interaction between unperturbed charges of the deformed reactants, $\Delta E_{\text{solute, Pauli}}$ accounts for the repulsion between occupied orbitals, $\Delta E_{\text{solute, oi}}$ is responsible for interaction between occupied and unoccupied orbitals and polarization. The ASM and EDA

terms were projected on the N1/N2–H bond stretch, as this geometrical parameter is critically involved in the reaction and undergoes a well-defined change^[9] over the course of the oxidative addition step.

Figure 2a shows that the interaction energies ($\Delta E_{\text{solute, int}}$) control the reaction regiochemistry, whereas the strain energy required for deformation of catalyst (Rh-L2) and substrate (one of the two 1,2,3-benzotriazole tautomers, **1a/b**) during oxidative addition ($\Delta E_{\text{solute, strain}}$) is nearly identical for both N1- (black) and N2-selective (red) pathways. Similar $\Delta E_{\text{solute, strain}}$ curves is a consequence of breaking the same N–H bond at either N1 or N2 during the oxidative addition. Because the $\Delta E_{\text{solute, int}}$ is decisive in determining the trend in ΔE_{solute} and thus the observed reactivity trends, it was further analyzed by using the EDA, and the results are plotted in Figure 2b. Differences in the orbital-interaction curves ($\Delta E_{\text{solute, oi}}$) are minimal. Thus, it becomes evident that the predominance of the N2-selective pathway can be attributed to the more stabilizing electrostatic interaction ($\Delta V_{\text{solute, elstat}}$), which effectively overrules the less destabilizing Pauli repulsion ($\Delta E_{\text{solute, Pauli}}$) preference for the N1 pathway.

Next, to understand the trend in $\Delta V_{\text{solute, elstat}}$ we examined the electrostatic potential maps (ESP) and Hirshfeld charges^[10] of Rh and N1, N2, N3 atoms of 1,2,3-benzotriazole fragments (**1a/b**). Figure 2c and d illustrate the ESP and charge analysis for the 1,2,3-benzotriazole tautomers at their equilibrium and TSs geometries. Our analysis has identified a causal relationship between the charge of the N atom of the benzotriazole involved in the regiodetermining oxidative addition step and the degree of electrostatic stabilization: a more electronegative N atom leads to a stronger, more stabilizing electrostatic interaction with the electropositive Rh metal center. Thus, the more reactive tautomer **1a** has an N1 atom positioned between a

carbon atom and nitrogen N2. This results in a relatively electronegative N1 (−36 ma.u.), which leads to a strongly stabilizing electrostatic interaction with Rh (20 ma.u.) metal center (Figure 2c). In contrast, the less reactive tautomer **1b** has a partially positive (44 ma.u.) N2 atom (Figure 2d) as a result of being positioned between two nitrogens (N1 and N3 atoms). This leads to less stabilizing electrostatic interaction between the N2 atom and the electropositive Rh. The electrostatic interactions are more stabilizing for the reaction of N2 compared with N1 over the entire reaction coordinate (Figure 2b), thus this charge and molecular electrostatic potential (MEP) analysis can be performed at any point.

In summary, we have computationally analyzed the reaction mechanism of a newly developed coupling of 1,2,3-benzotriazoles with allenes catalyzed by Rh-diphosphine ligand (JoSPOphos/DPEphos) complexes. Our DFT calculations reveal that regardless of the ligand being used, the reaction proceeds via a three-step catalytic cycle, comprised of first an oxidative addition, then hydrometalation, and finally a reductive elimination. Our activation strain and energy decomposition analyses on the regiodetermining oxidative addition step catalyzed by Rh-DPEphos show that the preference for the N2-selective reaction channel arises from a previously unrecognized electronic mechanism, namely, a more stabilizing electrostatic interaction between the electron-enriched region at the N1 atom of tautomer **1a** with the positively charged Rh during N1–Rh bond formation in the rate-determining N1–H oxidative addition step. We envisage that the newly identified electrostatic interactions can be used to further tune the 1,2,3-benzotriazole and catalyst interaction through the introduction of various functionalities, which may allow new reactions with tailored N2 regioselectivity trend.

Acknowledgements

T.S. is grateful to the P.R.I.M.E. fellowship funded by German Federal Ministry of Education and Research (BMBF) and the European Union (EU/FP7/Marie Curie Actions/COFUND). Calculations were performed on the Cartesius cluster supported by Dutch National High Performance Computing center SURFsara; Comet cluster operated by Extreme Science and Engineering Discovery Environment (XSEDE) through allocation TG-DMR110088. XSEDE is supported by National Science Foundation grant number ACI-1548562. We thank the Nederlandse Organisatie voor Wetenschappelijk Onderzoek (NWO) for financial support.

Conflict of interest

The authors declare no conflict of interest.

Keywords: activation strain analysis • allylation • DPEphos ligands • N–H activation • rhodium

[1] For selected reviews, see: a) L. Huang, M. Arndt, K. Gooßen, H. Heydt, L. J. Gooßen, *Chem. Rev.* **2015**, *115*, 2596–2697; b) P. Koschker, B. Breit,

- Acc. Chem. Res.* **2016**, *49*, 1524–1536; c) H. J. Davis, R. J. Phipps, *Chem. Sci.* **2017**, *8*, 864–877; d) L. Ping, D. S. Chung, J. Bouffard, S. Lee, *Chem. Soc. Rev.* **2017**, *46*, 4299–4328.
- [2] a) W. Roth, D. Spangenberg, Ch. Janzen, A. Westphal, M. Schmitt, *Chem. Phys.* **1999**, *248*, 17–25; b) N. Jagerovic, M. L. Jimeno, I. Alkorta, J. Elguero, R. M. Claramunt, *Tetrahedron* **2002**, *58*, 9089–9094; c) L. T. Ueno, R. O. Ribeiro, M. S. Rocha, M. E. V. Suárez-Iha, K. Iha, F. B. C. Machado, *J. Mol. Struct.* **2003**, *664*, 207–215; d) J. Poznański, A. Najda, M. Bretner, D. Shugar, *J. Phys. Chem. A* **2007**, *111*, 6501–6509.
- [3] N1-selective strategies: a) N. Arnau, Y. Arredondo, M. Moreno-Mañas, R. Pleixats, M. Villarroya, *J. Heterocycl. Chem.* **1995**, *32*, 1325–1334; b) W. Yan, X. Ye, K. Weise, J. L. Petersen, X. Shi, *Chem. Commun.* **2012**, *48*, 3521–3523; c) S. Gupta, N. Chandna, A. K. Singh, N. Jain, *J. Org. Chem.* **2018**, *83*, 3226–3235. N2-selective strategies: d) A. R. Katritzky, W. Kuzmierkiewicz, J. V. Greenhill, *Recl. Trav. Chim. Pays-Bas.* **2010**, *110*, 369–373; e) J. Wen, L. L. Zhu, Q.-W. Bi, Z.-Q. Shen, X.-X. Li, X. Li, Z. Wang, Z. Chen, *Chem. Eur. J.* **2014**, *20*, 974–978; f) K. Wang, P. Chen, D. Ji, X. Zhang, G. Xu, J. Sun, *Angew. Chem. Int. Ed.* **2018**, *57*, 12489–12493; *Angew. Chem.* **2018**, *130*, 12669–12673; g) L.-L. Zhu, L. Tian, H. Zhang, L. Xiao, W. Luo, B. Cai, H. Wang, C. Wang, G. Liu, C. Pei, Y. Wang, *Adv. Synth. Catal.* **2019**, *361*, 1117–1123.
- [4] a) I. Briguglio, S. Piras, P. Corona, E. Gavini, M. Nieddu, G. Boatto, A. Carta, *Eur. J. Med. Chem.* **2015**, *97*, 612–648; b) P. Worthington in *Bioactive Heterocyclic Compound Classes: Agrochemicals* (Eds.: C. Lamberth, J. Dinges), Wiley-VCH, New York, **2012**, pp. 129–145; c) Y. Cui, Y. Wu, X. Lu, X. Zhang, G. Zhou, F. B. Miapheh, W. Zhu, Z.-S. Wang, *Chem. Mater.* **2011**, *23*, 4394–4401.
- [5] K. Xu, N. Thieme, B. Breit, *Angew. Chem. Int. Ed.* **2014**, *53*, 7268–7271; *Angew. Chem.* **2014**, *126*, 7396–7399.
- [6] H. Landert, F. Spindler, A. Wyss, H.-U. Blaser, B. Pugin, Y. Ribourduoille, B. Gschwend, B. Ramalingam, A. Pfaltz, *Angew. Chem. Int. Ed.* **2010**, *49*, 6873–6876; *Angew. Chem.* **2010**, *122*, 7025–7028.
- [7] Geometry optimizations and frequency analysis were performed in Gaussian 09^[11] at the B3LYP-D3^[12] level of theory with a mixed basis set of LANL2DZ^[13] ECP for Rh and 6-31G(d)^[14] for other atoms in implicit solvent DCE treated with SMD solvation model.^[15] Single-point energies were computed at B3LYP-D3 level of theory with the SDD^[16] basis set for Rh, and 6–311 + +G(d,p) for the other atoms in DCE. Gibbs free energies are reported at 80 °C and a standard state of 1 mol L^{−1}. Grimme's quasi-harmonic approximation was used to compute the entropic contributions to the Gibbs free energies.^[17] To understand the factors governing reaction regioselectivity the activation strain model (ASM)^[9] and energy-decomposition analysis (EDA) were applied using ADF.2017.103^[18] and PyFrag programs^[19] at ZORA^[20]-B3LYP-D3/TZ2P^[21] on SMD(DCE)-B3LYP-D3/6-31G(d)/LANL2DZ geometries. To reduce computational cost, the cyclohexyl group of the allene (**2**) was replaced by the methyl (**2'**).
- [8] U. Gellrich, A. Meißner, A. Steffani, M. Kähny, H.-J. Drexler, D. Heller, D. A. Plattner, B. Breit, *J. Am. Chem. Soc.* **2014**, *136*, 1097–1104.
- [9] For reviews on the activation strain analysis, see: a) F. M. Bickelhaupt, K. N. Houk, *Angew. Chem. Int. Ed.* **2017**, *56*, 10070–10086; *Angew. Chem.* **2017**, *129*, 10204–10221; b) L. P. Wolters, F. M. Bickelhaupt, *WIREs Comput. Mol. Sci.* **2015**, *5*, 324–343; c) I. Fernández, F. M. Bickelhaupt, *Chem. Soc. Rev.* **2014**, *43*, 4953–4967; for the activation strain analysis in the condensed phase, see: d) T. A. Hamlin, B. van Beek, L. P. Wolters, F. M. Bickelhaupt, *Chem. Eur. J.* **2018**, *24*, 5927–5938.
- [10] B. J. Levandowski, T. A. Hamlin, H. J. Eckvahl, F. M. Bickelhaupt, K. N. Houk, *J. Mol. Model.* **2019**, *25*, 33/1–5.
- [11] M. J. Frisch et al. Gaussian 09, Revision D.01, Gaussian Inc.: Wallingford, CT, **2009**.
- [12] a) A. D. Becke, *J. Chem. Phys.* **1993**, *98*, 5648–5652; b) C. Lee, W. Yang, R. G. Parr, *Phys. Rev. B: Condens. Matter Mater. Phys.* **1988**, *37*, 785–789; c) A. D. Becke, *J. Chem. Phys.* **1993**, *98*, 1372–1377; d) P. J. Stephens, F. J. Devlin, C. F. Chabalowski, M. J. Frisch, *J. Phys. Chem.* **1994**, *98*, 11623–11627; e) T. Sperger, I. A. Sanhueza, I. Kalvet, F. Schoenebeck, *Chem. Rev.* **2015**, *115*, 9532–9586; f) S. Grimme, J. Antony, S. Ehrlich, H. Krieg, *J. Chem. Phys.* **2010**, *132*, 154104–154119.
- [13] L. E. Roy, P. J. Hay, R. L. Martin, *J. Chem. Theory Comput.* **2008**, *4*, 1029–1031.

- [14] a) R. Ditchfield, W. J. Hehre, J. A. Pople, *J. Chem. Phys.* **1971**, *54*, 724–728; b) W. J. Hehre, R. Ditchfield, J. A. Pople, *J. Chem. Phys.* **1972**, *56*, 2257–2261.
- [15] A. V. Marenich, C. J. Cramer, D. G. Truhlar, *J. Phys. Chem. B* **2009**, *113*, 6378–6396.
- [16] a) U. Häussermann, M. Dolg, H. Stoll, H. Preuss, P. Schwerdtfeger, R. M. Pitzer, *Mol. Phys.* **1993**, *78*, 1211–1224; b) W. Küchle, M. Dolg, H. Stoll, H. Preuss, *J. Chem. Phys.* **1994**, *100*, 7535–7542.
- [17] a) I. Funes-Ardoiz, R. S. Paton, *Goodvibes: Goodvibes v2.0.1*, **2016**, <http://doi.org/10.5281/zenodo.595246>; b) S. Grimme, *Chem. Eur. J.* **2012**, *18*, 9955–9964.
- [18] a) G. te Velde, F. M. Bickelhaupt, E. J. Baerends, C. Fonseca Guerra, S. J. A. van Gisbergen, J. G. Snijders, T. Ziegler, *J. Comput. Chem.* **2001**, *22*, 931–967; b) C. Fonseca Guerra, J. G. Snijders, G. te Velde, E. J. Baerends, *Theor. Chem. Acc.* **1998**, *99*, 391–403; c) ADF2017, SCM Theoretical Chemistry; Vrije Universiteit, Amsterdam, The Netherlands, <http://www.scm.com>.
- [19] X. Sun, T. M. Soini, J. Poater, T. A. Hamlin, F. M. Bickelhaupt, *J. Comput. Chem.* **2019**, *40*, 2227–2233.
- [20] a) E. van Lenthe, E. J. Baerends, J. G. Snijders, *J. Chem. Phys.* **1994**, *101*, 9783–9792; b) E. van Lenthe, R. van Leeuwen, E. J. Baerends, J. G. Snijders, *Int. J. Quantum Chem.* **1996**, *57*, 281–293.
- [21] E. van Lenthe, E. J. Baerends, *J. Comput. Chem.* **2003**, *24*, 1142–1156.

Manuscript received: November 26, 2019

Accepted manuscript online: November 28, 2019

Version of record online: February 4, 2020